# Departure of Nitrogen Bubbles at the Solid–Liquid Interface during the Solidification of Duplex Stainless Steels

Qian Wang [1,2,3], Chenyang Xing [1,2,3], Rui Wang [1,2,3], Peng Luo [1,2,3], Bo Wang [1,2,3,*], Jieyu Zhang [1,2,3] and Jie Ma [4,*]

1 State Key Laboratory of Advanced Special Steel, Shanghai University, Shanghai 200072, China
2 Shanghai Key Laboratory of Advanced Ferrometallurgy, Shanghai University, Shanghai 200072, China
3 School of Materials Science and Engineering, Shanghai University, Shanghai 200072, China
4 School of Materials and Chemical Engineering, Anhui Jianzhu University, Hefei 230601, China
* Correspondence: bowang@shu.edu.cn (B.W.); majie726@163.com (J.M.)

**Abstract:** The departure of nitrogen bubbles from duplex stainless steel (DSS) is essential for studying the precipitation behavior of bubbles during solidification. In the current work, the numerical and theoretical derivation of analytical formula were used to study the bubble departure at the solid–liquid interface. In the paper, the departure radius of bubbles was deduced by numerical analysis. Based on the works of subcooled boiling flow, the forces of bubbles were analyzed at the solid–liquid interface. The critical condition of bubble departure was theoretically obtained. The effects of various factors on bubble departure and slip were also analyzed. The results showed that the critical radius of the bubble departure increased at the solid–liquid interface when reducing the interface inclination angle, the depth of liquid steel, the contact angle, the flow velocity of liquid steel, and the gas pressure on the surface of liquid steel. Moreover, when the interface inclination angle equaled zero, there was no slip in the interface direction before bubble departure, letting the bubbles float directly. However, when the interface inclination angle equaled $\pi/4$ or $\pi/2$, the bubbles slid along the interface before bubble departure in the x negative direction, which was more likely to cause the bubbles to be trapped.

**Keywords:** duplex stainless steels; solidification; nitrogen bubbles; departure; slip

## 1. Introduction

Duplex stainless steel is a kind of stainless steel with a ferritic structure as the matrix and an austenitic structure as the second phase, and DSS has the characteristics of two kinds of stainless steel (ferritic stainless steel and austenitic stainless steel). DSS has been widely used as a functional integrated material with excellent performance. One of the future development trends is economical duplex stainless steel, which replaces nickel with nitrogen. However, due to the formation of single-phase ferrite at the initial stage of solidification, the solubility of nitrogen decreases, and then the gas escapes, causing pores and defects, which cannot be ignored.

The precipitation process of nitrogen bubbles in DSS is firstly due to the nucleation of nitrogen bubbles in the supersaturated region formed by the segregation phenomenon. When the nitrogen bubbles grow to a critical size, the force is large enough for the departure of the nitrogen bubbles from the nucleation surface. Furthermore, the bubbles then float in the liquid steel under the action of the force. These bubbles would probably be trapped at the solidification front and form gas pores, seriously affecting the quality of the product [1–6], In order to improve the quality of duplex stainless steels and reduce costs, studying the force of bubbles and analyzing the bubble departure phenomenon during solidification are both of importance.

In 1930s, Fritz [6] proposed a semi-empirical formula of the critical diameter of the bubble separation in the liquid layer through experimental and theoretical analysis when the departure force of the bubble is equal to the adhesion force.

$$D_d = 0.0208\theta \left[ \frac{\sigma}{\left(\rho_L - \rho_g\right)g} \right]^{0.5} \tag{1}$$

where $D_d$ is the departure diameter of bubbles, m; $\rho_L$ is the density of the liquid, $kg/m^3$; $\rho_g$ is the density of the gas, $kg/m^3$; g is gravity acceleration, $m/s^2$; $\theta$ is the contact angle; and $\sigma$ is the surface tension, N/m. Cole et al. [7] considered the effect of system pressure on the departure diameter of bubbles and proposed prediction models for the departure diameter of bubbles under different system pressures P, $N/m^2$:

$$D_d = \frac{1000}{P}\left[ \frac{\sigma}{\left(\rho_L - \rho_g\right)g} \right]^{0.5} \tag{2}$$

Svyazhin et al. [8] suggested that the formation of nitrogen bubbles during solidification is mainly determined by the desorption rate of nitrogen bubbles on the melted surface. Klausner et al. [9] established force balance equations for bubbles in the horizontal and vertical directions at the solid–liquid interface, respectively, and considered the effects of heat flux and mass flow rate on the departure of bubbles. There is often a period of slip along the wall surface before departure from the interface, and it is predicted that the critical diameter of the bubbles is close to the experimentally determined value.

Yu Zhijia et al. [10] studied the momentum equation of bubbles on a horizontal wall based on the study of bubbles on a vertical wall, considering the internal pressure force of the bubbles and the resistance force of the liquid during bubble growth. The equation of the bubble growth rate and bubble departure diameter was also established and verified by experimental methods. Yeoh et al. [11] and Yun et al. [12] researched the departure of bubbles considering the forces on a vertical wall. Meanwhile, Sugrue et al. [13] modified the functional relationship of the bubble growth rate and the contact relationship between the bubble and the interface on a declining wall based on the Klausner model and the Yun model and researched the critical dimension of bubble desorption on the wall as well.

In our previous work, we investigated the effect of the pressure in the bubbles, nitrogen solubility, nitrogen segregation, and casting parameters on the formation and growth of bubbles during solidification in the manufacturing of DSS [14]. The critical nucleation radius of nitrogen and the bubble growth rate equation in the liquid phase at the solid–liquid interface during solidification were derived. When the nitrogen bubbles grow to a critical size, the forces acting on the bubbles are large enough for departure from the solidification front. In this paper, the forces acting on the bubbles were analyzed at the solid–liquid interface based on the force of bubble departure in subcooled boiling conditions. The force equations of the bubble departure and slip were also established, as well as the effects of various factors such as the interface inclination angle, contact angle, the flow velocity of molten steel, and gas pressure on the surface of the molten steel on the departure of bubbles. Matlab and C/C++ languages were also used to calculate all kinds of equations.

## 2. Theory Basis

At the solid–liquid interface, due to the diffusion of nitrogen atoms, nitrogen atoms in the solid phase and the liquid phase continuously diffuse into the bubbles, causing the bubbles to grow. According to the force analysis shown in Figure 1, when the resultant force of the bubble in all directions on the solid–liquid interface is zero, the bubble will desorb [9,13,15]; the force parallel to the solid–liquid surface only changes the sliding of bubbles on the surface. Therefore, the critical condition of bubble departure is the resultant force of the bubble in the normal direction of the interface being zero at the solid–liquid

interface. Figure 1 shows the schematic diagram of bubble departure at the solid–liquid interface during solidification.
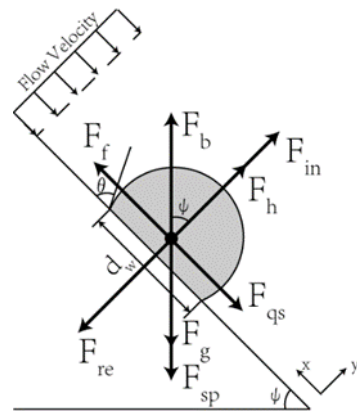


**Figure 1.** A schematic diagram of bubble departure at the solid–liquid interface.

In Figure 1, $F_{in}$ is the internal pressure force, $F_{qs}$ is the drag force, $F_h$ is the hydrodynamic pressure, $F_{re}$ is the curvature-induced capillary force, $F_b$ is the buoyancy, $F_g$ is gravity, $F_{sp}$ is the static pressure of molten steel, and $F_f$ is the frictional resistance.

The assumptions of the bubble departure at the solid-liquid interface are proposed as follows:

1.  When the bubble is desorbed, the bubble is always spherical.
2.  The effect of temperature gradient on surface tension is not considered.
3.  The solid–liquid interface is planar, and the angle between the solid–liquid interface and the horizontal direction is φ.
4.  The flow velocity of molten steel at the solid–liquid interface is parallel to the wall.
5.  The force and motion of bubbles are not considered in the direction perpendicular to the paper.
6.  The velocity gradient of molten steel flowing parallel to the wall direction (x direction) is not considered.
7.  The effect of the bubble growth rate on bubble departure is not considered.

The forces of the bubble departure at the solid–liquid interface can be shown as:

(1)    Internal pressure force ($F_{in}$) [10]

Because the force of the gas inside the bubble to the wall and the wall to the gas is a mutual force, the direction of the interaction force is perpendicular to the wall. Therefore, the force acting on the wall inside the bubble is as follows:

$$F_{in} = P_b \frac{\pi}{4} d_w^2 \tag{3}$$

where, $P_b$ is gas pressure in the bubble, which can be expressed as follows:

$$P_b = P_0 + \rho_L gh + \frac{2\sigma_{LG}}{R} \tag{4}$$

where, $P_0$ is the gas pressure on the surface of the molten steel; $\rho_L g$ is the surface tension; $\rho_L$ is the density of molten steel; R is the bubble departure radius, m; g is gravitational acceleration; and h is the depth of the liquid steel, m; $d_w$ is the diameter of the circle of contact between the bubble and the wall, which can be calculated as:

$$d_w = 2R \sin \theta \tag{5}$$

where, θ is the contact angle.

(2)    Shear lift force ($F_{sL}$) [11]

When the bubble floats in the liquid, the velocity of the liquid near the wall is small and the hydrostatic pressure is large. Far away from the wall, the flow velocity is large, and the hydrostatic pressure is small, thus producing shear lift force. The force caused by the shear movement of the fluid is equivalent to the side-lift force perpendicular to the relative velocity of the liquid phase to the bubble in a velocity gradient flow field. It is closely related to the velocity gradient of molten steel flow, and the direction is perpendicular to the flow direction of molten steel. When the velocity gradient of liquid steel flow is not considered, the shear lift force can be neglected. The expression of shear lift force is as follows:

$$F_{sL} = \frac{1}{2} C_L \rho_L v_L^2 \pi R^2 \tag{6}$$

where, $C_L$ is the expression of the lift coefficient, which can be expressed as follows:

$$C_L = 0.8 G_s = 0.8 \left| \frac{dv}{dx} \right| \frac{R}{v} \tag{7}$$

where, $G_s$ is the dimensionless shear rate. As the velocity gradient in the boundary layer of the solid–liquid interface is small, according to assumption 6, the change in the velocity gradient in the x direction is not considered, that is, $dv/dx = 0$. Therefore, $C_L = 0$ and $F_{sL} = 0$.

(3)　Drag force ($F_{qs}$) [16]

When the liquid flows around the bubble at a certain speed, a pair of forces which are equal in value and of opposite direction are produced between the liquid and the bubble. The force acting on the bubble is called the drag force, which is given by:

$$F_{qs} = \frac{1}{2} C_D \rho_L v_L^2 \pi R^2 \tag{8}$$

where, $v_L$ is flow velocity of molten steel, m/s and $C_D$ is the drag coefficient, which is closely related to the Reynolds number (Re).

When Re ≤ 500,

$$C_D = \frac{24}{Re} \left( 1 + 0.1 Re^{0.75} \right) \tag{9}$$

When 500 ≤ Re ≤ 200,000,

$$C_D = \frac{4}{3} \left( \frac{g \left( \rho_L - \rho_g \right) R^2}{\sigma_{LG}} \right)^{0.5} \tag{10}$$

where, $\rho_g$ is the density of the bubble and Re is the Reynolds number, which can be expressed as follows:

$$Re = 2R \rho_L v_L / \eta_L \tag{11}$$

where, $\eta_L$ is the dynamic viscosity of molten steel.

(4)　Hydrodynamic pressure ($F_H$) [9,13]

The hydrodynamic pressure generated by the action of molten steel near the bubble can be shown as:

$$F_h = \frac{9}{8} \rho_L v_L^2 \frac{\pi d_w^2}{4} \tag{12}$$

(5)　Curvature-induced capillary force ($F_{re}$) [10]

The bubble is subjected to surface resistance of the liquid during bubble growth, which is called expansion resistance.

$$F_{re} = -8\pi \sigma_{LG} R \tag{13}$$

According to assumption 1, the influence of the flow on the shape of bubbles is not considered, so the direction of expansion resistance is perpendicular to the wall.

(6)　Buoyancy ($F_b$)

$$F_b = \frac{4}{3}\pi\rho_L R^3 g \tag{14}$$

(7)　Gravity ($F_g$)

$$F_g = -\frac{4}{3}\pi\rho_b R^3 g \tag{15}$$

(8)　Static pressure of molten steel ($F_{sp}$)

$$F_{sp} = -\rho_L g h \frac{\pi}{4}d_w^2 \tag{16}$$

(9)　Frictional resistance ($F_f$)

When the bubble is stationary at the solid–liquid interface, the frictional resistance of the interface to the bubble is parallel to the interface and opposite to the relative motion direction of the bubble.

$$F_f = \frac{\pi}{4}C_f P_b d_w^2 \tag{17}$$

where, $C_f$ is the local friction coefficient, which can be estimated from the Brahmas plate solution [17], and the expression is:

$$C_f = 0.664/Re^{1/2} \tag{18}$$

According to the analysis of the force at the time of bubble departure, the vector equation expression of the force acting on the bubble at the solid–liquid interface is:

$$\sum F = F_h + F_{in} + F_{re} + F_b + F_g + F_{sp} + F_{qs} + F_f \tag{19}$$

The analysis of the force in the x and y directions according to the above equation is as follows:

$$\sum F_x = F_b sin\varphi + F_g sin\varphi + F_{qs} + F_{sp} sin\varphi + F_f \tag{20}$$

$$\sum F_y = F_h + F_{in} + F_{re} + F_b cos\varphi + F_g cos\varphi + F_{sp} cos\varphi \tag{21}$$

According to Equations (20) and (21), when the resultant force in the y direction is greater than zero and the resultant force in the x direction is equal to zero, the bubble will disengage along the normal direction of the interface (y direction). When the resultant force in the y direction is greater than zero and the resultant force in the x direction is not equal to zero, the bubble will slide along the interface horizontally (x direction) before leaving the interface. When the resultant force in the x direction is not equal to zero and the resultant force in the y direction is less than or equal to zero, the bubble will only slide along the interface horizontally (x direction) without leaving the interface. The direction of slip is often the same as the resultant direction of the x direction. In conclusion, the resultant force in the y direction determines whether the bubble is detached from the interface. Meanwhile, the resultant force in the x direction determines whether the bubble slides in the direction along the solid–liquid interface.

## 3. Results and Discussion

According to the stress conditions of nitrogen bubbles on solid–liquid interface and Equations (20) and (21), Equation (21) can be simplified as:

$$\frac{9}{8}v_L^2 \sin^2\theta + \frac{P_0 R + \rho_L g h R + 3}{\rho_L}\sin^2\theta - \frac{12}{\rho_L R} + \frac{4}{3}Rg\cos\varphi - gh\cos\varphi\sin^2\theta = 0 \tag{22}$$

According to Equation (22), the size of a bubble departing from the solid–liquid interface is closely related to the interface inclination angle $\varphi$, the contact angle $\theta$, the depth

of liquid steel h, the flow velocity of liquid steel $v_L$, and the gas pressure $P_0$ on the surface of the liquid steel.

Under different conditions, the calculation parameters and solutions for the critical size of bubble departure were determined, as shown in Table 1. In addition, the influence of different factors on bubble departure was analyzed.

**Table 1.** The calculation parameters and solutions for the bubble departure radius.

| Parameters | Value |
|---|---|
| Contact angle, $\theta$ | $\pi/4$, $\pi/2$ |
| Interface inclination angle, $\varphi$ | 0, $\pi/4$, $\pi/2$ |
| Depth of molten steel, h (m) | 0.4, 0.7, 1.0, 2.0 |
| Flow velocity of liquid steel, $v_L$ (m·s$^{-1}$) | 0.02, 0.2, 1.0, 2.0 |
| Surface pressure of molten steel, $P_0$ (Pa) | 50,000, 100,000, 200,000 |

### 3.1. The Influence of the Interface Inclination Angle $\varphi$

The relationship between the radius of the bubble departure in the y direction and the interface inclination angle is shown in Figure 2. It demonstrates the situation when the contact angle $\theta = \pi/4$, the flow velocity of liquid steel is equal to 0.2 m·s$^{-1}$, and the gas pressure is equal to 100,000 Pa on the surface of the molten steel.
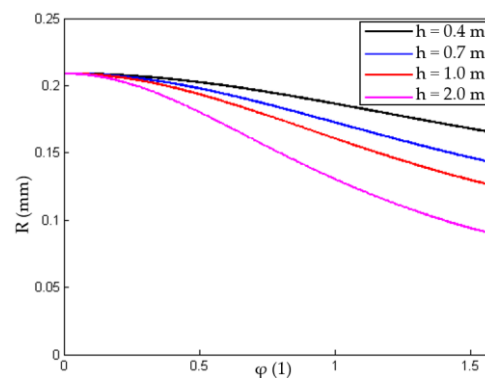


**Figure 2.** The relationship between the radius of the bubble departure in the y direction and the interface inclination angle at different depth of molten steel.

The relationship between the radius of the bubble departure and the depth of the molten steel in the y direction at different interface inclination angles is shown in Figure 3.
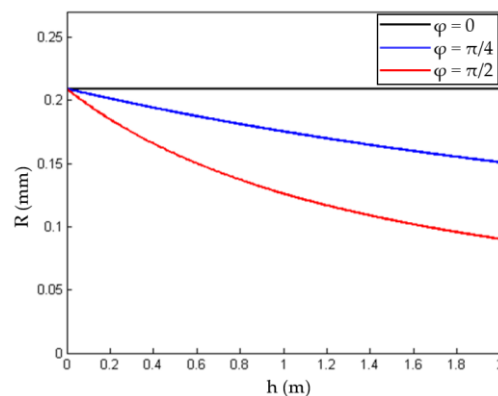


**Figure 3.** The relationship between the radius of the bubble departure and the depth of the molten steel in the y direction at different interface inclination angles.

When $\varphi = 0$, the bubble departure radius was constant (R = 0.209 mm) at different depth of liquid steel. At this point, the depth of the molten steel had no effect on the bubble departure radius at the horizontal interface. However, when the inclination angle was greater than zero, the bubble departure radius decreased with the increase in the molten steel depth. When the depth of liquid steel was constant, the bubble departure radius in the y direction decreased with the increase in the inclination angle. In addition, when $\varphi = \pi/2$, the radius of bubble departure was the smallest. Therefore, the smaller the interface inclination angle and the smaller the depth of molten steel, the larger the radius of bubble departure.

When the contact angle $\theta = \pi/4$, the flow velocity of liquid steel $v_L = 0.2$ m·s$^{-1}$, the gas pressure $P_0 = 100{,}000$ Pa, and the bubble departs from the interface in y direction. The friction resistance $F_f$ in the x direction (if its direction first keeps the positive direction of x) and the resultant force are shown in Table 2.

**Table 2.** The resultant forces in x direction when the bubble departs from the interface in y direction at different interface inclination angles and depths of molten steel.

| Inclination Angle $\varphi$ | Depth of Molten Steel h (m) | Departure Radius of Bubble in y Direction R (mm) | Frictional Resistance $F_f$ (N) | Resultant Force in x Direction $\sum F_x$ (N) |
|---|---|---|---|---|
| $\varphi = 0$ | 0.4 | 0.2093 | $5.0693 \times 10^{-4}$ | $4.9170 \times 10^{-4}$ |
| | 0.7 | 0.2093 | $5.7812 \times 10^{-4}$ | $5.6290 \times 10^{-4}$ |
| | 1.0 | 0.2093 | $6.4932 \times 10^{-4}$ | $6.3409 \times 10^{-4}$ |
| | 2.0 | 0.2093 | $8.8662 \times 10^{-4}$ | $8.7140 \times 10^{-4}$ |
| $\varphi = \pi/4$ | 0.4 | 0.1944 | $4.5732 \times 10^{-4}$ | $-6.6047 \times 10^{-4}$ |
| | 0.7 | 0.1845 | $4.8422 \times 10^{-4}$ | $-0.0013$ |
| | 1.0 | 0.1756 | $5.0660 \times 10^{-4}$ | $-0.0018$ |
| | 2.0 | 0.1512 | $5.5658 \times 10^{-4}$ | $-0.0028$ |
| $\varphi = \pi/2$ | 0.4 | 0.1658 | $3.6697 \times 10^{-4}$ | $-7.7969 \times 10^{-4}$ |
| | 0.7 | 0.1434 | $3.4132 \times 10^{-4}$ | $-0.0012$ |
| | 1.0 | 0.1264 | $3.2063 \times 10^{-4}$ | $-0.0013$ |
| | 2.0 | 0.0905 | $2.7137 \times 10^{-4}$ | $-0.0014$ |

When $\varphi = 0$, the direction of the friction resistance was the same as the direction of the resultant force, and the friction resistance was greater than the resultant force. Therefore, there was no slip in the direction of the interface when the bubble departs from the interface. When the interface inclination angle was $\pi/4$ and $\pi/2$, the direction of the friction resistance was opposite to the direction of the resultant force. In addition, the friction resistance was smaller than the resultant force. At this time, the bubble slips along the interface in the negative direction of x before departure.

### 3.2. The Influence of the Contact Angle θ

When the interface inclination angle $\varphi = \pi/2$, the flow velocity of liquid steel $v_L = 0.2$ m·s$^{-1}$ and the gas pressure $P_0 = 100{,}000$ Pa, and the relationship between the radius of the bubble departure in the y direction and the contact angle at the different depths of liquid steel are shown as Figure 4. The relationship between the radius of the bubble in the y direction and the depth of the molten steel at different contact angles are presented as Figure 5.

The radius of bubble departure increased with the decrease in the contact angle between the bubble and the interface. When the contact angle was small, the wettability between the bubble and the interface was poor, so the radius of the bubble was larger. In addition, the influence of the contact angle on the bubble departure radius was more significant at a greater depth of molten steel. Zhijia Yu et al. [18] concluded that with the increase in the liquid velocity, the contact angle of bubbles obviously increases, the liquid velocity increases, the drag force of liquid flow increases, and the inclination of bubbles increases.
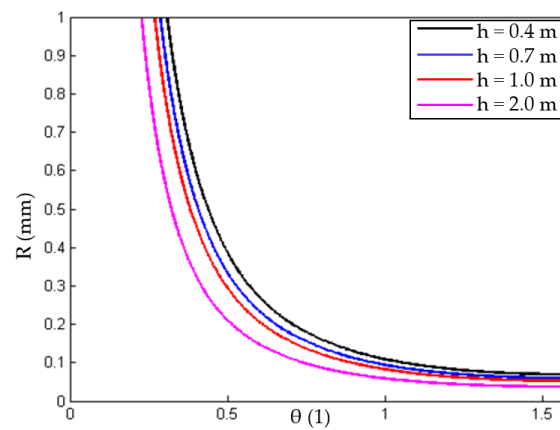
**Figure 4.** The relationship between the radius of the bubble departure in the y direction and the contact angle at the different depths of liquid steel.
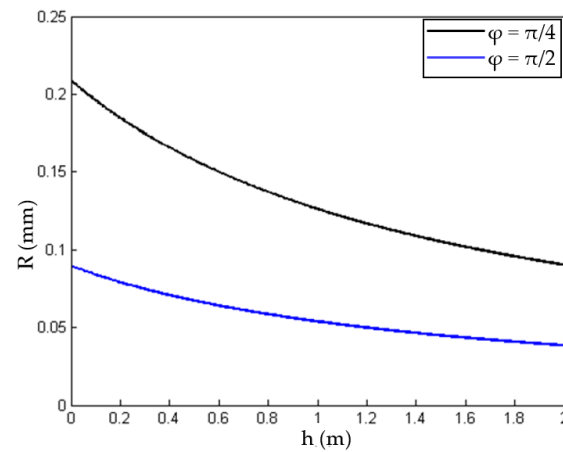


**Figure 5.** The relationship between the radius of the bubble in the y direction and the depth of the molten steel at different contact angles.

### 3.3. The Influence of the Flow Velocity of Liquid Steel $v_L$

When the interface inclination angle $\varphi = \pi/2$, the contact angle $\theta = \pi/4$ and the gas pressure $P_0 = 100,000$ Pa, and the relationship between the bubble departure radius in the y direction and the depth of molten steel at different flow velocities of liquid steel are shown as Figure 6.
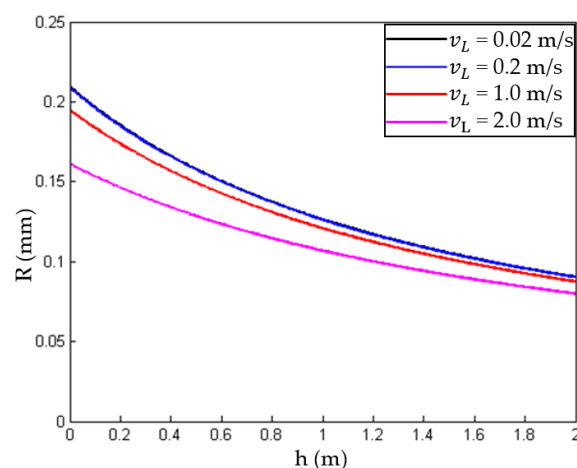


**Figure 6.** The relationship between the bubble departure radius in the y direction and the depth of molten steel at different flow velocities of liquid steel.

Under certain liquid steel depths, the dynamic pressure increased with the flow velocity of the liquid steel. However, the influence of the dynamic pressure was less than that of other forces when the change in the flow velocity of liquid steel was small. Therefore, when the flow velocity of liquid steel was from 0.02 m·s$^{-1}$ to 0.2 m·s$^{-1}$, the change in the bubble departure radius was not obvious. Compared with 0.02 m·s$^{-1}$, the change in the bubble departure radius was relatively more obvious under the situation when the flow velocity of the steel was 2.0 m·s$^{-1}$. Overall, reducing the flow velocity of liquid steel could increase the radius of the bubble departure. Zhijia Yu et al. [18] concluded that with the increase in liquid velocity, the detachment diameter of bubbles decreases, while the liquid velocity increases, and the drag force and shear lift acting on the bubbles increase, which promotes the early detachment of bubbles and reduces the detachment diameter of bubbles.

### 3.4. The Influence of the Gas Pressure $P_0$ on the Surface of the Molten Steel

When the interface inclination angle $\varphi = \pi/2$, the contact angle $\theta = \pi/4$ and the flow velocity of the liquid steel $v_L = 0.2$ m·s$^{-1}$, and the relationship between the bubble departure radius in the y direction and the depth of molten steel at different gas pressures are shown as Figure 7.
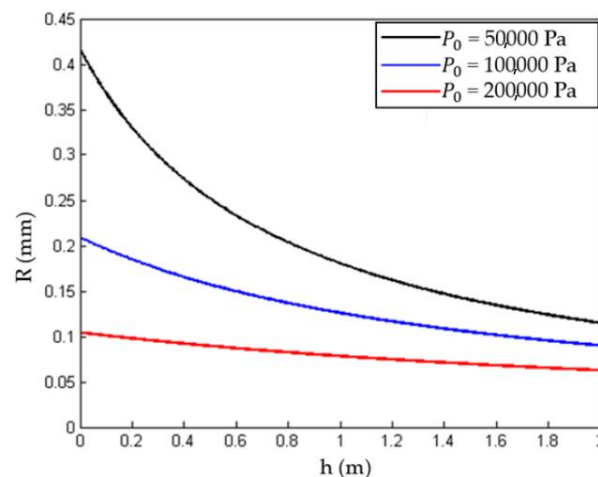


**Figure 7.** The relationship between the bubble departure radius in the y direction and the depth of molten steel at different gas pressures.

Under certain conditions, with the increase in the gas pressure on the surface of the molten steel, the internal pressure of the bubble and the resultant force of the bubble departure increased, and it was easier for it to precipitate out from the interface. Therefore, the radius of the bubble departure in the direction of the interface (y direction) decreased. Meanwhile, when the gas pressure on the surface of molten steel was higher, the influence of the depth of molten steel on the bubble departure radius in the y direction became weaker.

### 4. Conclusions

The slip and departure of bubbles were determined by the forces acting on the bubbles in the x and y directions, respectively. The equation of the critical departure radius is as follows:

$$\frac{9}{8}v_L^2 \sin^2\theta + \frac{P_0 R + \rho_L ghR + 3}{\rho_L}\sin^2\theta - \frac{12}{\rho_L R} + \frac{4}{3}Rg\cos\varphi - gh\cos\varphi\sin^2\theta = 0 \quad (23)$$

Decreasing the interface inclination angle or the depth of molten steel increased the radius of bubble departure under certain conditions. When the depth of the molten steel was constant, the wetting angle between the bubble and the interface decreased, which reduced the wettability between them, and this then increased the radius of the bubble departure; the increase in the velocity of the liquid steel made the dynamic pressure larger,

which reduced the departure radius of the bubbles. Under certain conditions, the increase in the gas pressure on the surface of the molten steel increased the pressure inside the bubble, thus enlarging the resultant force on the bubble. A greater resultant force will cause the bubble to depart at a smaller radius. The bubble radius influences the floatation speed of the bubble, which further determines whether the bubble will be trapped or not.

Under the condition that $\sum F_y = 0$ when the interface inclination angle was equal to zero, there was no slip in the interface direction before bubble departure, causing the bubble to float directly. When the interface inclination angle was equal to $\pi/4$ or $\pi/2$, the bubble slid along the interface before bubble departure. The direction of slip was the negative x direction. The longer the slip time of the bubble, the more likely the bubble is to remain in the DSS.

**Author Contributions:** Conceptualization, Q.W. and B.W.; methodology, B.W. and J.M.; software, C.X. and Q.W.; validation, Q.W. and B.W., formal analysis, R.W., C.X. and Q.W.; investigation, C.X., Q.W., J.M. and B.W.; resources, B.W.; data curation, B.W. and J.M.; writing—original draft preparation, J.Z. and B.W.; writing—review and editing, P.L., Q.W. and B.W.; visualization, B.W.; supervision, B.W.; project administration, B.W. and J.Z.; funding acquisition, B.W. and J.Z. All authors have read and agreed to the published version of the manuscript.

**Institutional Review Board Statement:** Not applicable.

**Informed Consent Statement:** Not applicable.

**Data Availability Statement:** Data presented in this article are available on request from the corresponding author.

**Conflicts of Interest:** The authors declare no conflict of interest.

# References

1. Nickens, H.V.; Yannitell, D.W. The effects of surface tension and viscosity on the rise velocity of a large gas bubble in a closed, vertical liquid-filled tube. *Int. J. Multiph. Flow* **1987**, *13*, 57–69. [CrossRef]
2. Lin, S.Y.; Wang, W.J. Systematic effects of bubble volume on the surface tension measured by pendant bubble profile. *Colloids Surf. A Physicochem. Eng. Asp.* **1996**, *114*, 31–39. [CrossRef]
3. Kang, Y.T.; Nagano, T. Mass transfer correlation of $NH_3$-$H_2O$ bubble absorption. *Int. J. Refrig.* **2002**, *25*, 878–886. [CrossRef]
4. Prodanovic, V.D.; Fraser, D. Bubble Behavior in Subcooled Flow Boiling of Water at Low Pressures and Flow Rates. *Int. J. Multiph. Flow* **2002**, *28*, 1–19. [CrossRef]
5. van Sint Annaland, M.; Deen, N.G. Numerical simulation of gas bubbles behaviour using a three-dimensional volume of fluid method. *Chem. Eng. Sci.* **2005**, *60*, 11. [CrossRef]
6. Fritz, W. Berechnung des maximal volumens von Dampfblasen. *Phys. Z.* **1935**, *36*, 379–384.
7. Cole, R.; Shulman, H.L. Bubble departure diameters at subatmospheric pressures. *Chem. Eng. Prog. Symp. Ser.* **1966**, *62*, 6–16.
8. Svyazhin, A.G.; Kaputkina, L.M. Phases and defects upon the solidification of nitrogen-alloyed stainless steels. *Phys. Met. Metallogr.* **2015**, *116*, 552–561. [CrossRef]
9. Klausner, J.F.; Mei, R. Vapor Bubble Departure in Forced Convection Boiling. *Int. J. Heat Mass Transf.* **1993**, *36*, 651–662. [CrossRef]
10. Kaptay, G. Classification and general derivation of interfacial forces, acting on phases, situated in the bulk, or at the interface of other phases. *J. Mater. Sci.* **2005**, *40*, 2125–2131. [CrossRef]
11. Yeoh, G.H.; Tu, J.Y. A unified model considering force balances for departing vapour bubbles and population balance in subcooled boiling flow. *Nucl. Eng. Des.* **2005**, *235*, 1251–1265. [CrossRef]
12. Yun, B.J.; Splawski, A. Prediction of a Subcooled Boiling Flow with Advanced Two-Phase Flow Models. *Nucl. Eng. Des.* **2012**, *253*, 351–359. [CrossRef]
13. Sugrue, R.; Buongiorno, J. A Modified Force-Balance Model for Prediction of Bubble Departure Diameter in Subcooled Flow Boiling. *Nucl. Eng. Des.* **2016**, *305*, 717–722. [CrossRef]
14. Dai, K.; Wang, B.; Xue, F.; Liu, S.; Huang, J.; Zhang, J. Formation of nitrogen bubbles during solidification of duplex stainless steels. *Metall. Mater. Trans. B* **2018**, *49*, 2011–2021. [CrossRef]

15. Raj, S.; Pathak, M. An Analytical Model for Predicting Growth Rate and Departure Diameter of a Bubble in Subcooled Flow Boiling. *Int. J. Heat Mass Transf.* **2017**, *109*, 470–481. [CrossRef]

16. Ishii, M.; Zuber, N. Drag coefficient and relative velocity in bubbly, droplet or particulate flows. *AIChE J.* **1979**, *25*, 843–855. [CrossRef]

17. Probstein, R.F. *Physicochemical Hydrodynamics: An Introduction*; John Wiley & Sons: Hoboken, NJ, USA, 2005.

18. Yu, Z.; Sun, C.; Zhao, Z.; Sun, X.; Qi, W. Research on Bubble Dynamics of Liquid Flow Boiling in Vertical Rectangular Channel. *J. Eng. Thermophys.* **2001**, *3*, 354–358.